 doi:10.20944/preprints202208.0500.v1

Article

Experimental Proof-Of-Concept of a Spatial Photonic Switch Based on an Off-Axis Zone Plate in Millimeter Wavelength Range

A.G. Paulish,[1,2,3] Yu.E. Geints,[4,] O.V. Minin,[5,6] I.V. Minin[5,6]

[1] Rzhanov Institute of Semiconductor Physics SB RAS, 630090, Novosibirsk, Russia; paulish@corp.nstu.ru
[2] Novosibirsk State Technical University, 630073, Novosibirsk, Russia; paulish@corp.nstu.ru
[3] Novosibirsk State University, 630090, Novosibirsk, Russia; paulish@corp.nstu.ru
[4] V.E. Zuev Institute of Atmospheric Optics, SB RAS; ygeints@iao.ru
[5] National Research Tomsk State University, 634050, Tomsk, Russia; oleg.minin@ngs.ru
[6] Siberian State University of Geosystems and Technologies, 630010, Novosibirsk, Russia; prof.minin@gmail.com
* Correspondence: paulish@corp.nstu.ru , A.P.

Abstract: Optical switches are a key element in modern network communications. We present the results of experimental verification of a new theoretical concept proposed earlier for a full-optical wavelength-selective dual-channel switch based on the photonic hook effect, which is free from using any micro-mechanical devices or nonlinear materials. A large-scale laboratory prototype of such a device based on an off-axis Wood zone plate is considered and its main parameters in the millimeter wavelength range are investigated On the basis of the experiments, we show that the optical isolation of switched channels for a switch based on an off-axis zone plate can achieve 15 dB at a frequency difference of 25 GHz in frequency range from 93 to 136 GHz. Given the scaling, these results can be transferred to another range, including the optical one.

Keywords: optical switch; photonic hook; off-axis zone plate

1. Introduction

The significant growth of data communications and the rapid development of dense wavelength-division multiplexing (DWDM) technology are creating the need for more robust and flexible signal management capabilities. In particular, the ability to optimize, route, and communicate data using optical methods is becoming critical. Optical switches are used in modern optical network communications [1], in particular to separate optical signals with different frequencies propagating over a single optical channel.

Modern requirements for device microminiaturization dictate the need for developing the optical components and systems "on-a-chip" because fast real-time reconfiguration using integrated optical circuit technologies will ensure energy-efficient and transparent data transmission and switching at high speed (in contrast to switching circuits based on electronics, which require control of an external electrical signal) [2]. Optical switches are also widely used for "neuromorphic" optical computing, simulating brain functions to parallel information processing and storage [3].

Different principles of optical switches design are known nowadays [1,2,4-8]. The most common are the switches based on mirrors or lenses, which mechanically rotates or changes its configuration to provide optical switching [9-12]. The main drawback of these switches is their rather low speed. Another class of switches includes wavelength-selective switches [13-16], which have attracted much attention because of their ability to independently route channels with different wavelengths. This better suit for the modern photonic networks which must perform multiplexing and routing using only

 doi:10.20944/preprints202208.0500.v1

optical technologies based on the properties of optical radiation with different wavelengths.

Worth mention is also the family of wavelength-division multiplexing (WDM) multiplexers based on the generation of whispering-gallery modes in transparent microspheres [17-18].

The physical principle underlying the previously proposed concept of non-contact spectrally selective switching of optical channels [19] is based on the effect of a curvilinear photonic flux generation during propagation of an optical wave through a specific diffractive optical element with wavelength-scale dimensions. This class of devices belongs to the family of wavelength-selective switches [1,2]. In principle, the creation of a curvilinear photonic flux (a photonic hook) can be achieved in several ways. One of them is to use an optically homogeneous particle, but having an asymmetry of geometric shape or using the asymmetry of the illuminating beam. For example, it can be a rectangular prism, a cylinder [20,21] or an ellipsoid under side illumination [22], an asymmetric planar lens in the form of a mesowavelength off-axis phase plate [23], etc. Another method of producing a curved photonic flux exploits the geometrically symmetrical microparticles, but having a specially created asymmetry of the refractive index [20]. These are, the so-called, Janus particles obtained by combining together two or more materials with different optical properties [24].

An important feature of a photonic hook which enables the realization the function of an optical switch is the dependence of the curvature of produced photonic jet on the optical wavelength. Therefore, with a certain spatial configuration of the photonic switch and properly chosen receiving angles, it is possible to achieve a change in the optical signals in each switching channel as the radiation wavelength changes, without using mechanical scanning systems or nonlinear material properties.

In this communication, we present the results of the experimental proof of the concept of above-mentioned optical switch in the millimeter (MM) wavelength range fabricated as a scaled-up version of the optical switch due to linearity of Maxwell's equations. To realize the optical switching function, the required dependence of the curvature angle of the focused radiation on the irradiation wavelength is provided by a diffractive element in the form of a zone plate. Specifically, the spatial tilt of the near-field focusing region is provided by using an off-axis Wood zone plate (WZP) providing the focusing outside the optical axis of the system.

2. Materials and Methods

Scheme of the experimental setup, its main components and operation principle are shown in Figures 1 and 2. MM radiation is generated by the source (1), passes through a waveguide (2) to a Cassegrain antenna (3) producing a quasi-planar electromagnetic wave (5) with the diameter $D \approx 100$ mm which exposes the phase plate (6). The distance d from the Cassegrain antenna to the WZP is much greater than the working aperture of the antenna D, i.e. the far-field conditions are realized. After the WZP, the MM radiation (7) is focused in the plane ZX, located outside the optical axis of the incident radiation (5). Depending on the radiation frequency, the beam focusing position is shifted along the Z axis in the ZX plane. To measure the spatial distribution of the radiation intensity in the ZX plane, the photodetector (8–10) is placed in the center of a bi-directional mounting stage with the electromechanical drives controlled by the computer. Coordinate scanning of the focusing region is carried out by the photodetector within the area of 100×100 mm with the spatial step of 0.5 mm.

The radiation source (Figure 2a) is a monolithic Gann diode-based MM radiation module with operating frequencies of 93, 118 and 136 GHz (tuning range ± 0.75 GHz) and output power of 3, 1 and 0.2 mW, respectively. The MM modules are equipped with a waveguide terminating in a Cassegrain antenna. The antenna provides a quasi-planar wave front with a radiation beam divergence of less than 1º.

Preprints (www.preprints.org) | NOT PEER-REVIEWED | Posted: 30 August 2022 doi:10.20944/preprints202208.0500.v1

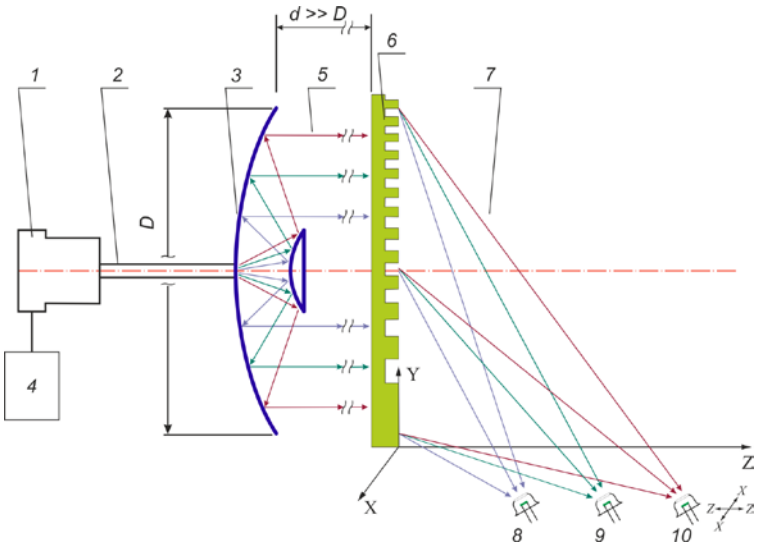

Figure 1. Experimental setup: MM emitter (1), waveguide (2), Cassegrain antenna (3), control board (4), incoming quasi-parallel MM beam (5), off-axis Wood zone plate (6), focused MM beam (7), photodetector positions on different switching channels (8, 9, 10).

(**a**) (**b**) (**c**)

Figure 2. (**a**) Appearance of MM radiation source, consisting of (1) MM emitter, (2) waveguide, (3) Cassegrain antenna and (4) control board; (**b**) Pyroelectrical photodetector for the MM waveband; (**c**) Image of a Wood zone plate.

As a MM radiation sensor, the pyroelectric photodetector (see, the appearance in Figure 2b) based on tetraaminodiphenyl with an extended range of spectral sensitivity (0.4-3000 μm) is used. The photodetector has an input window of polyethylene terephthalate with a diameter of 5 mm and a photosensitive pad with the area of 1×1 mm^2. The characteristics of the used pyroelectric photodetector are studied in detail in [25,26]. To obtain the maximum signal from the pyroelectric detector, the MM radiation is modulated with a frequency of about 100 Hz using a mechanical obturator.

An asymmetric photonic structure in the form of an off-axis binary Wood phase plate [23,27] is used as an optical switching element, as shown in Figure 2c. WZP with the diameter D_W = 120 mm is fabricated by 3D printing [28] on a Cheap3d V300 printer with a printing area of 300×300×300 mm, with an accuracy of 50 μm. The material used is an ABS plastic REC rod with a diameter of 1.75 mm. The refractive index of the material according to the data [29] is $n \approx 1.59$ and can be slightly varied by choosing the density of 3D printing [30]. Note that at such geometrical parameters of the mesoscale WZP, the Mie-size parameter of the structure is $q = \pi D_W / \lambda = 31\ \pi$ that falls into the range of the photonic jet effect manifestation [31].

Preprints (www.preprints.org) | NOT PEER-REVIEWED | Posted: 30 August 2022 doi:10.20944/preprints202208.0500.v1

3. Results

The results of the experiments are shown in Figures 3,4, and Table 1. Figure 3 shows the two-dimensional distribution of MM wave intensity experienced the diffraction on the WZP for three selected frequencies from 93 to 136 GHz. Note, this distribution is a synthesis of the spatial distributions of MM radiation obtained for each frequency separately.

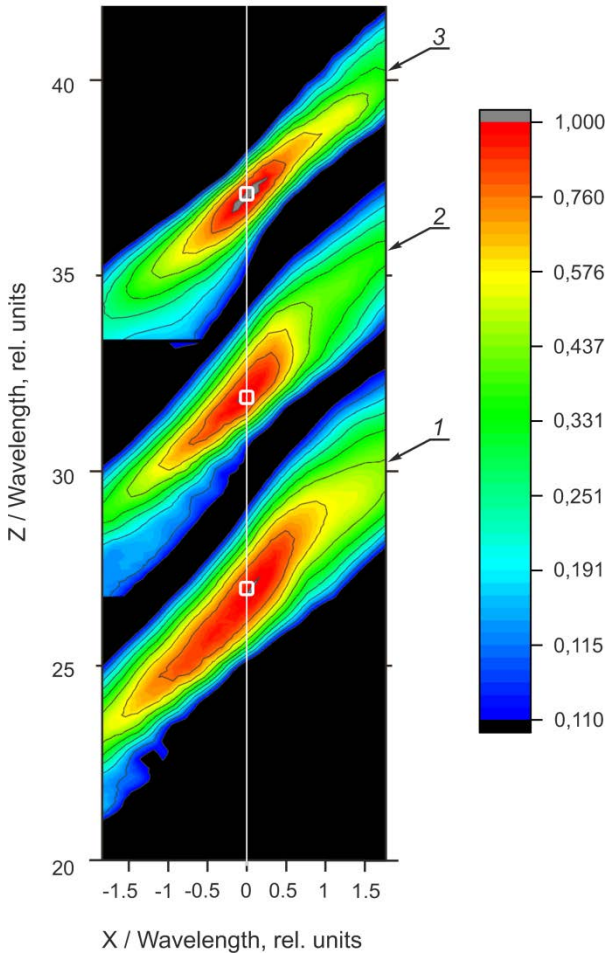

Figure 3. MM intensity distribution in ZX-plane at the frequencies (1) 93, (2) 118 and (3) 136 GHz. X and Z coordinates are normalized to the radiation wavelength. Squares show the boundaries of the photosensitive area of the pyroelectric receiver.

Table 1. The parameters of MM radiation intensity *z*-distribution for different switching channels.

Frequency (GHz)	Wavelength (mm)	Maximum coordinate, Z / λ (rel. units)	FWHM, ΔZ / λ (rel. units)	FWHM, ΔZ / Z (%)
93	3,23	26,9	2,29	8,5
118	2,54	31,8	1,86	5,8
136	2,21	37,1	1,56	4,2

Preprints (www.preprints.org) | NOT PEER-REVIEWED | Posted: 30 August 2022 doi:10.20944/preprints202208.0500.v1

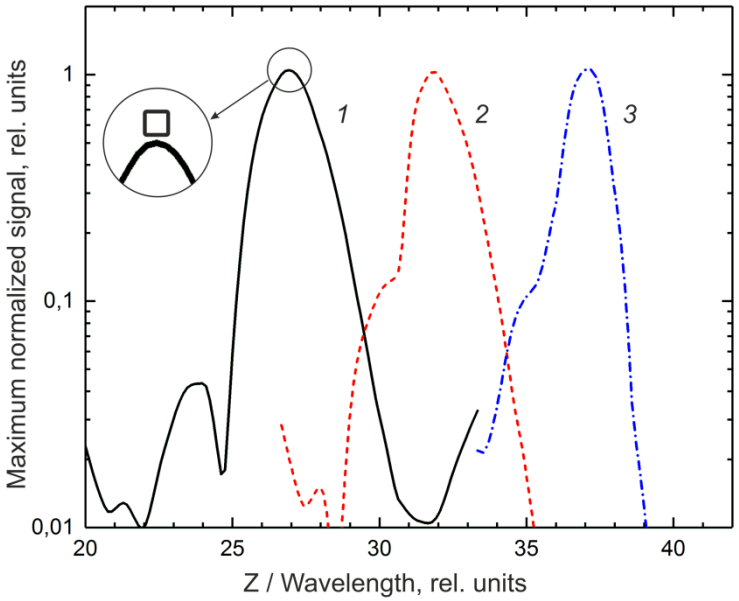

Figure 4. Dependence of MM radiation intensity along the optical axis Z (shown in Fig. 3 by a solid line) at the frequencies 93, 118 and 136 GHz. The values are normalized to the maximum obtained for each frequency separately. Z coordinate is normalized to the radiation wavelength. *Inset*: The photosensitive pad of the pyro-receiver (open square) shown in scale of the figure data.

4. Discussion

From these figures is seen, that as expected due to wave diffraction, the spatial size of the focusing region changes when the MM radiation propagates away from WZP. This is detailed in Table 1. Meanwhile, the electromagnetic wave localization region (off-axis focus [23,27]) changes its spatial position when the radiation wavelength changes. The placement of optical receivers along the Z axis at X = 0 provides different field amplitude in each of the switching channels when operating at different frequencies, i.e. enables the spatial switching by the magnitude of the optical signal. Obviously, the operation reliability of such a switch depends on the value of optical decoupling of the channels, which in turn depends on the parameters of the switching phase plate and the irradiation wavelength range. The difference of electric signals from neighboring receivers, $dS = S_1 - S_2$, serves as a merit of the optical isolation (decoupling) of the switching channels. Note that to improve the optical decoupling of the switched channels, we have chosen a photodetector with an input aperture much smaller than the size of the cross section of the radiation localization region (see Figure 4 *Inset*).

Figure 4 shows the intensity distribution of refracted MM radiation along the Z-axis at X = 0 for different frequencies. In this figure, MM intensity is normalized to its maximal value obtained for each frequency, while Z-coordinates are normalized to the radiation wavelength. The boundaries of photosensitive area of pyroelectric photodetector are shown by a square in the inset in relative coordinates. The results of statistical processing of the obtained dependences are presented in Table 1. From Fig. 4 one can see that the MM radiation intensity at the frequency 118 GHz, if measured at the coordinate of the signal maximum for 93 GHz, is more than 15 times lower than the maximal radiation intensity with a frequency of 93 GHz. In other words, the measured mutual influence of the intensity levels at adjacent frequencies is less than 15 dB.

Importantly, such value of the radiation isolation dS of the switching routes is a good result provided that the switch response speed is near instantaneous as, for example, for the photodetectors based on Schottky diodes ZBD-F (Virginia Diodes, the response time is about 3×10^{-11}s [32]). In this case, the spectral range of switching realization is about 43 GHz, that is about 38% of the average wavelength.

5. Conclusions

To conclude, we experimentally demonstrate the principal possibility of creating a multichannel (in this case, a three-channel) optical switch based on a dielectric mesowavelength diffraction element with broken geometric symmetry in the form of an off-axis Wood zone plate. Due to the unique property of such diffraction structure to change the spatial position of the diffraction-limited focusing region depending on the radiation wavelength, this switch is a good candidate for implementing electronic optical commutation in modern optoelectronics, which does not require control of an electrical signal. Worth noting, no full-scale optimization of the optical switch characteristics is intended in this work and only the proposed earlier concept is experimentally demonstrated. Moreover, given the scalability of Maxwell's equations, the results of this work can be transferred to other ranges of electromagnetic radiation, in particular, to optical or infrared wavelength bands.

Author Contributions: Experiment preparation: A.P.; Conceptualization, I.M. and O.M.; formal analysis, I.M., O.M., A.P., Y.G.; investigation, I.M., O.M., A.P.; writing—original draft preparation, review and editing: I.M., O.M.; translation, Y.G.; supervision, I.M., O.M.; All authors have read and agreed to the published version of the manuscript.

Funding: This research was funded by RFBR (No. 21-57-10001), Ministry of Science and Higher Education of the Russian Federation (V.E. Zuev Institute of Atmospheric Optics SB RAS).

Conflicts of Interest: The authors declare no conflict of interest.

Acknowledgement: This work was supported by Tomsk Polytechnic University Development Program.

References

1. El-Bawab T.S.; *Optical Switching*, Springer, Boston, MA, 2006.
2. Stabile R.; Albores-Mejia A.; Rohit A. et al. Integrated optical switch matrices for packet data networks. *Microsyst Nanoeng* 2016, *2*, p. 15042.
3. Cheng Z.; Ríos C.; Pernice W. H. P.; Wright C. D.; Bhaskaran H. On-chip photonic synapse *Sci. Adv.* **2017**, *3(9),* e1700160.
4. Cheng Q.; Bahadori M.; Glick M.; Rumley S. and K. Bergman. Recent advances in optical technologies for data centers: a review *Optica* **2018**, *5*, pp. 1354–1370.
5. Virgilio M.; Witzigmann B.; Bolognini G.; Guha S.; Schroeder T. and G. Capellini. CMOS-compatible optical switching concept based on strain-induced refractive-index tuning. *Opt. Express* **2015**, *23*, pp. 5930-5940.
6. Ravel K.; Koechlin C.; Prevost E.; Bomer T.; Poirier R.; Tonck L.; Guinde G.; Beaumel M.; Parsons N.; Enrico M. and S. Barker. Optical switch matrix development for new concepts of photonic based flexible telecom payloads. In Proceedings of SPIE 11180, International Conference on Space Optics — ICSO 2018, Chania, Greece, 9-12 October 2018, 111803H.
7. Jia H.; Yang S.; Zhou T.; Shao S.; Fu X.; Zhang L. and Yang L. WDM-compatible multimode optical switching system-on-chip *Nanophotonics* **2019**; *8(5)*, pp. 889–898.
8. Williamson I.A.D. and Fan S. Broadband Optical Switch based on an Achromatic Photonic Gauge Potential in Dynamically Modulated Waveguides *Phys. Rev. Applied* **2019**, *11*, p. 054035.
9. Li L.; Liu C.; Peng H.; Wang Q. Optical switch based on electrowetting liquid lens. *J. Appl. Phys.* **2012**, *111*, pp. 103103.
10. Seok T. J.; Quack N.; Han S.; Muller R. S.; Wu M. C. Large-scale broadband digital silicon photonic switches with vertical adiabatic couplers. *Optica* **2016**, *3*, pp. 64–70.
11. Han S.; Seok T. J.; Quack N.; Yoo B.-W.; Wu M. C. Large-scale silicon photonic switches with movable directional couplers. *Optica* **2015**, *2*, pp. 370–375.
12. S. Han, T. J. Seok, K. Yu, N. Quack, R. S. Muller, and M. C. Wu. Large-scale polarization-insensitive silicon photonic MEMS switches. *J. Lightwave Technol.* **2018**, *36*, pp. 1824–1830.
13. T. J. Seok, J. Luo, Z. Huang, K. Kwon, J. Henriksson, J. Jacobs, L. Ochikubo, R. S. Muller, and M. C. Wu. Silicon photonic wavelength cross-connect with integrated MEMS switching. *APL Photonics* **2019**, *4*, p. 100803.
14. Han S.; Seok T. J.; Quack N.; Yoo B.-W.; Wu M. C. Large-scale silicon photonic switches with movable directional couplers. *Optica* **2015**, *2*, p. 370.
15. Strasser T. A. and Wagener J. L. Wavelength-selective switches for ROADM applications. *IEEE J. Sel. Top. Quantum Electron*. **2010**, *16*, pp. 1150–1157.
16. Zhang C.; Zhang M.; Xie Y.; Shi Y.; Kumar R.; Panepucci R. R.; Dai D. Wavelength-selective 2 × 2 optical switch based on a Ge2Sb2Te5-assisted microring. *Photon. Res*. **2020**, *8*, pp. 1171-1176.

17. Grujic K.; Hole J.P.; Hellesø O.G.; Wilkinson J.S. (2006) Whispering gallery modes excitation in borosilicate glass microspheres by K+ ion-exchanged channel waveguide coupler. In Proceedings of SPIE: Photonics West: 8th International Conference on Laser Beam Control and Applications, San José, Costa Rica, 22 - 26 Jan 2006.
18. Işçi S.; Bilici T.; Kurt A.; Serpengüzel A. Morphology-dependent resonances of optical microsphere resonators for the realization of passive wavelength-division multiplexing components. *Opt. Eng.* **2004**, *43(5)*, pp. 1051-1055.
19. Geints Y.; Minin I.V.; Minin O.V. Concept of a miniature photonic spatial switch based on an off-axis zone plate. *Quantum Electronics* **2021**, *51(8)* pp. 727–729.
20. Geints Y.; Minin I.V.; Minin O.V. Tailoring 'photonic hook' from Janus dielectric microbar. *J. Opt.* **2020**, *22*, p. 065606.
21. Minin I.V.; Minin O.V.; Liu C.; Wei H.; Geints Y.; Karabchevsky A. Experimental demonstration of a tunable photonic hook by a partially illuminated dielectric microcylinder. *Optics Letters* **2020**, *45(17)*, pp. 4899-4902.
22. Liu C.; Chung H.; Minin O.V.; Minin I.V. Shaping photonic hook via well-controlled illumination of finite-size graded-index micro-ellipsoid. *J. Opt.* **2020**, *22(8)*, p. 085002.
23. Minin I.V.; Minin O.V.; Golodnikov D.O. Simple free-space method for measurement of dielectric constant by means of diffractive optics with new capabilities. In Proceedings of 8th International Conference on Actual Problems of Electronic Instrument Engineering, Novosibirsk, Russia, 26-28 Sept. 2006, p. 3-8.
24. Su H.; Hurd Price H.; Jing L.; Tian Q.; Liu J.; Qian K. Janus particles: design, preparation, and biomedical applications. *Materials Today Bio* **2019**, *4*, p. 100033.
25. Paulish A. G.; Gusachenko A. V.; Morozov A. O.; Dorozhkin K. V.; Suslyaev V. I.; Golyashov V. A.; Minin O. V.; Minin I. V. Characterization of tetraaminediphenyl-based pyroelectric detector from visible to millimeter wave ranges. *Optical Engineering* **2020**, *59(6)*, p. 061612.
26. Paulish A. G.; Gusachenko A. V.; Morozov A. O.; Golyashov V. A.; Dorozhkin K. V.; Suslyaev V. I. Sensitivity of the tetraaminodiphenyl based pyroelectric sensor from visible to sub-THz range. *Sensor Review* **2020**, *40(3)*, pp. 291–296.
27. Guo Y. J. and Barton S. K. Offset Fresnel zone plate antennas. *Int. J. of Satellite Communications* **1994**, *12(4)*, pp. 381-385.
28. Monkevich J. M. and Le Sage G. P. 'Design and fabrication of a customdielectric Fresnel multi-zone plate lens antenna using additive manufacturing techniques. *IEEE Access* **2019**, *7*, pp. 61452–61460.
29. Furlan W. D.; Ferrando V.; Monsoriu J. A.; Zagrajek P.; Czerwińska E.; Szustakowski M. 3D printed diffractive terahertz lenses. *Opt. Lett*. **2016**, *41*, pp. 1748-1751.
30. Poyanco J.M.; Pizarro F.; Rajo-Iglesias E. Cost-effective wideband dielectric planar lens antenna for millimeter wave applications. *Sci Rep*. **2022**, *12*, p. 4204.
31. Minin I.V.; Minin O.V.; Geints Y.E. Localized EM and photonic jets from non-spherical and non-symmetrical dielectric mesoscale objects: Brief review. *Annalen der Physik (Berlin)* **2015**, *527(7–8)*, pp. 491-497.
32. Fast Detectors (ZBD-F). Available online: https://vadiodes.com/en/zbd (accessed on 02 August 2022).